Journal of Hazardous Materials 178 (2010) 333–340

Contents lists available at ScienceDirect

Journal of Hazardous Materials

journal homepage: www.elsevier.com/locate/jhazmat

Adsorption of copper(II) on multiwalled carbon nanotubes in the absence and presence of humic or fulvic acids

Guodong Sheng[a,b], Jiaxing Li[b], Dadong Shao[b], Jun Hu[b], Changlun Chen[b,*], Yixue Chen[a], Xiangke Wang[a,b,*]

[a] School of Nuclear Science and Engineering, North China Electric Power University, Beijing, 102206, PR China
[b] Key Laboratory of Novel Thin Film Solar Cells, Institute of Plasma Physics, Chinese Academy of Sciences, P.O. Box 1126, Hefei, 230031, PR China

ARTICLE INFO

Article history:
Received 18 June 2009
Received in revised form 18 January 2010
Accepted 19 January 2010
Available online 25 January 2010

Keywords:
MWCNTs
Cu(II)
Adsorption
HA
FA

ABSTRACT

The adsorption of Cu(II) on multiwalled carbon nanotubes (MWCNTs) as a function of pH and ionic strength in the absence and presence of humic acid (HA) or fulvic acid (FA) was studied using batch technique. The results indicated that the adsorption is strongly dependent on pH but independent of ionic strength. A positive effect of HA/FA on Cu(II) adsorption was found at pH <7.5, whereas a negative effect was observed at pH >7.5. The adsorption isotherms can be described better by the Freundlich model than by the Langmuir model in the absence and presence of HA/FA. Adsorption isotherms of Cu(II) at higher initial HA/FA concentrations are higher than those of Cu(II) at lower FA/HA concentrations. The thermodynamic data calculated from temperature-dependent adsorption isotherms suggested that the adsorption was spontaneous and enhanced at higher temperature. Results of this work suggest that MWCNTs may be a promising candidate for the removal of heavy metal ions from aqueous solutions.

1. Introduction

Since their discovery by Iijima in 1991 [1,2], carbon nanotubes (CNTs) have attracted great attention because of their unique hollow tube structure and their many remarkable and outstanding mechanical, electronic, chemical and optical properties [3–8]. CNTs have been proposed for a large number of applications such as hydrogen storage devices, flat-panel displays, chemical sensors, microelectronic devices, catalyst supports, and so forth [9,10]. Due to their large surface area and high reactivity, CNTs have been widely used as superior solid phase extractors or adsorbents for the preconcentration and removal of various organic and inorganic pollutants from water [11–16].

In previous studies, extensive experiments have been conducted on the adsorption of heavy metal ions or organic contaminants on CNTs [13,14], and it was reported that CNTs possess higher adsorption capacity and show better reversibility through many cycles of water treatment and regeneration than that of commercial adsorbents, suggesting that CNTs are promising adsorbents for the removal of heavy metal ions or organic contaminants from large volumes of aqueous solutions regardless of their high unit cost at the present time [17,18]. However, there is little information with respect to the effect of organic contaminants on the adsorption of heavy metals and vice versa, while it should be realized that heavy metal ions and organic contaminants may present simultaneously at many contaminated sites [19,20]. For example, the presence of natural organic matter (NOM), such as humic acid (HA) and fulvic acid (FA), may influence the adsorption of heavy metal ions on CNTs in natural environment. Therefore, it is significant to study the adsorption behaviors of heavy metal ions on CNTs in the presence of organic contaminants and vice versa.

NOM exists ubiquitously in natural aquatic environments, with two of its main fractions as HA and FA. CNTs would readily interact with NOM upon contact [21–24]. As the consequence of these interactions, the surface properties of CNTs would be altered, thus affecting the adsorption of environmental contaminants by CNTs [24]. In recent studies, Hyung et al. [21,22] reported that NOM interacted strongly with CNTs and formed stable complexes in aqueous solutions. It was also observed that the adsorptive interaction was dependent on the types of NOM and proportional to the aromatic carbon contents of NOM. However, according to our literature survey, influence of the bound NOM on the adsorptive behavior of heavy metal ions to CNTs has not been examined.

In this work, we investigated the adsorption of Cu(II) on multiwalled carbon nanotubes (MWCNTs) in the absence and presence of HA or FA. Cu(II) was selected as a model heavy metal ion because of its extensive existence in water environment. The basic objectives of the present work are: (1) to investigate the

* Corresponding authors at: Key Laboratory of Novel Thin Film Solar Cells, Institute of Plasma Physics, Chinese Academy of Sciences, P.O. Box 1126, Hefei, 230031, PR China. Tel.: +86 551 5592788.
E-mail addresses: clchen@ipp.ac.cn (C. Chen), xkwang@ipp.ac.cn (X. Wang).

0304-3894/$ – see front matter © 2010 Elsevier B.V. All rights reserved.
doi:10.1016/j.jhazmat.2010.01.084

Table 1
^{13}C NMR characteristics (chemical shift ppm) of HA and FA.

	0–50	51–105	106–160	161–200	Aromaticity
HA	15	21	47	17	57
FA	16	28	19	39	30

adsorption kinetics and to analyze the experimental data with the pseudo-second-order equation; (2) to study the adsorption of Cu(II) on MWCNTs by varying experimental conditions, i.e., pH, ionic strength, HA/FA concentrations, addition sequences; (3) to investigate the adsorption thermodynamic and isotherms and to analyze experimental data with the Langmuir and Freundlich models.

2. Experimental process

2.1. Materials

MWCNTs were prepared by using chemical vapor deposition (CVD) of acetylene in hydrogen flow at 760 °C using Ni-Fe nanoparticles as catalysts [25]. $Fe(NO_3)_2$ and $Ni(NO_3)_2$ were treated by the sol–gel process and calcinations to obtain FeO and NiO and then deoxidized by H_2 to achieve Fe and Ni nanoparticles. Oxidized MWCNTs were prepared by oxidization with 3 mol L^{-1} HNO_3 [26]. Briefly, 400 mL 3 mol L^{-1} HNO_3 including 2 g of MWCNTs was ultrasonically stirred for 24 h, filtrated, and then rinsed with doubly distilled water until the pH reached about 6. Such prepared sample was dried overnight in an oven at 80 °C, and then calcined at 450 °C for 4 h to completely remove nitrate ions and amorphous carbon [27]. The catalysts Fe and Ni in the oxidized MWCNTs were measured by ICP–MS and the results indicated that Ni and Fe were less than 0.01% and 0.03%, respectively.

HA and FA were extracted from the soil of Hua-Jia county (Gansu province, China) [28–30]. Cross-polarization magic angle spinning (CPMAS) ^{13}C NMR spectra of HA and FA were divided into four chemical shift regions, i.e., 0–50 ppm, 51–105 ppm, 106–160 ppm, and 161–200 ppm. These regions were referred to as aliphatic, carbohydrate, aromatic, and carboxyl regions. The percentage of total intensity for each region is calculated by integrating the CPMAS ^{13}C NMR spectra with each region, and the fraction of aromatic groups calculated by expressing aromatic C as percentage of the sum of aliphatic C (0–105 ppm) + aromatic C (106–160 ppm) is listed in Table 1. HA and FA have also been characterized as a suite of 3 discrete acids with pK_a values listed in Table 2. The concentrations of functional groups of HA and FA determined by fitting the potentiometric titration data using FITEQL 3.1 are given in Table 2. The weight-averaged molecular weights (M_w) of dissolved HA and FA are determined according to the method of Chin et al. [31], and the M_w values of dissolved HA and FA are calculated to be 2108 and 1364, respectively.

All chemicals were purchased in analytical purity and were used without further purification. Milli-Q water was used in all experiments. The Cu(II) stock solution was prepared by dissolving $Cu(NO_3)_2$ in Milli-Q water and then diluted to 60 mg L^{-1}.

2.2. Characterization

The morphology of MWCNTs was characterized by a field emission scanning electron microscope (FE-SEM, JEOL JSM-6700, Tokyo, Japan) and a high-resolution transmission electron microscope (HR-TEM, JEOL JEM-2010, Tokyo, Japan). Fourier transform infrared (FTIR) technique was used in the analysis of the chemical surface groups of the adsorbents. FTIR analysis was performed using a Nexus670 FTIR spectrometer (Thermo Nicolet, Madison) equipped with a KBr beam splitter (KBr, FTIR grade). Spectra were acquired in the 4000–400 cm^{-1} wavenumber with 4 cm^{-1} resolution. The background spectrum of KBr was also recorded at the same conditions. The structural information of MWCNTs was evaluated by a Raman Spectrometer (Model Nanofinder 30R., Tokyo Instruments Inc., Tokyo, Japan).

2.3. Adsorption experiments

Duplicate batches were examined to prepare adsorption curves and to study the characteristics of adsorption process. The relative errors of the data were about ±5%.

Firstly, adsorption kinetic experiments were performed in a 500 mL conical flask, at predetermined time intervals, 5 mL of supernatant solutions was pipetted from the conical flask, and then separated after ultracentrifugation at 18,000 rpm (i.e., 31,152 × g) for 20 min. The residual Cu(II) concentration in the solution was determined by ICP-AES (Perkin-Elmer). For pH and ionic-strength effect experiments, the adsorption of Cu(II) on MWCNTs was investigated using batch experiments. The pH of the systems was adjusted by addition of 0.1 or 0.01 mol L^{-1} HNO_3 or NaOH.

Adsorption isotherms were investigated by using batch technique in polyethylene centrifuge tubes under ambient conditions at 293, 313, and 333 K, respectively. The stock solutions of 0.01 mol L^{-1} $NaNO_3$ and 1.0 g L^{-1} MWCNTs were pre-equilibrated for 5 h before the addition of Cu(II) stock solution. The initial concentrations of Cu(II) were from 1.0 to 20.0 mg L^{-1}. The samples were gently shaken for 2 days (which was enough to achieve equilibrium).

To take into account of Cu(II) loss for Cu(II) adsorption on tube wall, calibration curves were obtained separately under otherwise identical conditions as the adsorption process but without MWCNTs. Based on the obtained calibration curves, the amount of Cu(II) adsorbed on MWCNTs was calculated by subtracting the mass in the solution from the mass spiked.

3. Results and discussion

3.1. Characterization of MWCNTs

The scan electron microscope (SEM) and transmission electron microscope (TEM) images of oxidized MWCNTs are shown in Figure SI-1. The oxidized MWCNTs have very smooth surfaces and cylindrical shapes with 1–10 μm long and 10–30 nm outer diameter. N_2 adsorption–desorption isotherms and the corresponding BJH pore-size distribution curve of the MWCNTs are shown in Figure SI-2A and 2B, respectively. The stepwise adsorption and desorption isotherms are indicative of 3D intersection of a solid porous

Table 2
The concentrations of functional groups of HA and FA calculated from potentiometric titration by using FITEQL 3.1.

	$\log K_a$			C (mol g^{-1})[a]			Surface sites density (mol g^{-1})	WSOS/DF
	L_1	L_2	L_3	HL_1	HL_2	HL_3		
HA	−5.04	−7.40	−9.60	2.20×10^{-3}	1.08×10^{-3}	3.18×10^{-3}	6.46×10^{-3}	2.37
FA	−5.19	−7.77	−10.53	1.83×10^{-3}	1.08×10^{-3}	2.42×10^{-2}	2.71×10^{-2}	0.10

[a] HL_1, HL_2 and HL_3 represent the carboxyl groups (–COOH), the phenolic groups (Ar–OH) and the amine groups ($-NH_2$) of HA and FA, respectively.

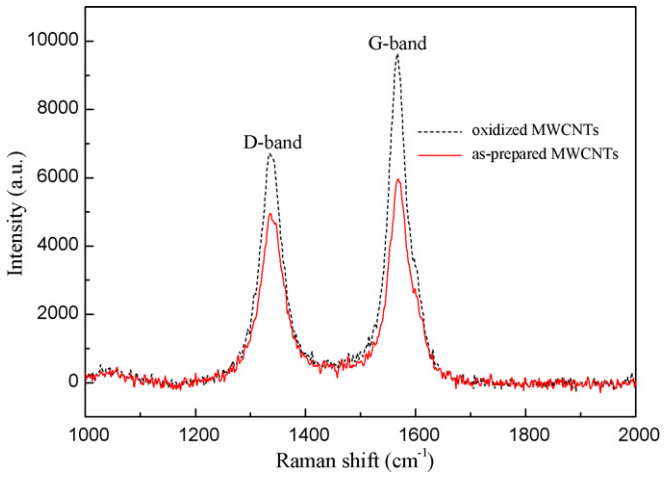

Fig. 1. Raman spectra of as-prepared and oxidized MWCNTs.

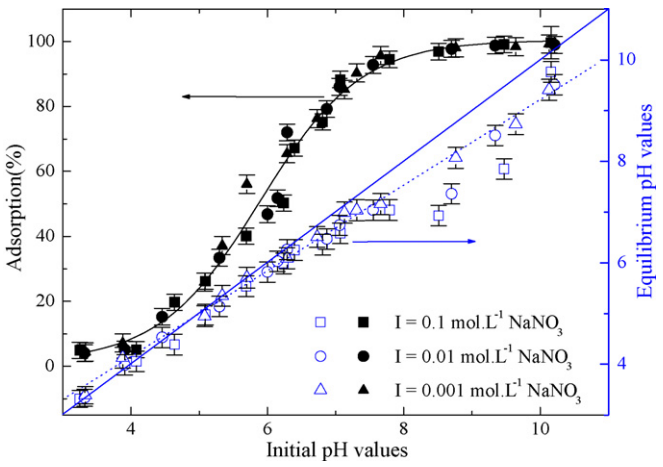

Fig. 2. Adsorption of Cu(II) on MWCNTs as a function of pH. MWCNT content = 1.0 g L^{-1}, initial Cu(II) concentration = 8.0 mg L^{-1}, T = 293 K. Solid points: adsorption vs. initial pH values; open points: equilibrium pH values vs. initial pH values.

material [32]. The specific surface area of the oxidized MWCNTs was 197 m^2 g^{-1} and the main pore inner diameter of the oxidized MWCNTs was 3.6 nm. Li et al. [33,34] had measured the surface area of MWCNTs and found that the MWCNTs oxidized with HNO_3 had a larger specific surface area than that of the untreated MWCNTs. The amorphous carbon, carbon nanoparticles, produced by the CVD method, was removed during the oxidation process using HNO_3. The FTIR spectrum (Fig. SI-3) indicates that the acid treatment process introduces many functional groups onto the surface of MWCNTs. The pH_{zpc} (zero point charge) value is measured to be 5.3 by using potentiometric titration (Fig. SI-4).

The Raman spectra of raw and oxidized MWCNTs presented in Fig. 1 are composed of two characteristic peaks. The peak near 1350 cm^{-1} is the D-band corresponding to the disordered sp^2-hybridized carbon atoms of nanotubes while the peak near 1580 cm^{-1} is the G-band corresponding to the structural integrity of sp^2-hybridized carbon atoms of nanotubes. Together, these bands can be used to evaluate the extent of carbon-containing defects [36]. As can be observed, the raw MWCNTs have a higher I_D/I_G ratio (the intensity ratio of D-band to G-band) than the oxidized MWCNTs. This suggests that the raw MWCNTs contain more amorphous carbon and multishell sp^2-hybridized carbon nanoparticles that can encapsulate residual metal catalysts. In other words, the raw MWCNTs have less crystalline graphitic structures.

3.2. Effect of pH and ionic strength

The pH dependence of Cu(II) adsorption on MWCNTs ranging from 3.0 to 10.0 at three different ionic strengths (i.e., 0.1, 0.01 and 0.001 mol L^{-1} $NaNO_3$) is shown in Fig. 2. As can be seen, the pH of the aqueous solution plays an important role to the adsorption of Cu(II) on MWCNTs. With the C_0 of 8 mg L^{-1}, the adsorption of Cu(II) on MWCNTs increases slowly at pH ranging from 3.0 to 5.3, then increases abruptly at pH 5.3–7.5 and at last maintains the high adsorption with increasing pH at pH >7.5. About 90% of Cu(II) is adsorbed on MWCNTs at pH >7.5.

It is well known that Cu(II) species can be present in aqueous solution in the forms of Cu^{2+}, $Cu(OH)^+$, $Cu(OH)_2$, $Cu(OH)_3^-$ and $Cu(OH)_4^{2-}$ [13]. At pH <7.5, the predominant Cu(II) species is always Cu^{2+} and the removal of Cu(II) is mainly accomplished by adsorption reaction. Therefore, the low Cu(II) adsorption that took place at low pH can be attributed in part to competition between H^+ and Cu^{2+} ions on the same sites [13]. Furthermore, as is mentioned above, the pH_{zpc} of MWCNTs is about 5.3. In the pH range lower than the pH_{zpc}, the surface charge of MWCNTs is positive and Cu(II) is hardly adsorbed on the surface of MWCNTs because of the electrostatic repulsion. Therefore, the removal percentage of Cu(II) is very low at pH <5.3. When pH value is higher than pH_{pzc}, the negative charged surface of MWCNTs provides electrostatic attraction that are favorable for the adsorption of cationic species, thus the adsorption of Cu(II) on MWCNTs increases abruptly at pH 5.3–7.5. In the pH range of 7.5–10.0, the removal of Cu(II) remains constant and reaches maximum. The main Cu(II) species are $Cu(OH)^+$, $Cu(OH)_2$, and $Cu(OH)_3^-$, and thus the removal of Cu(II) is possibly accomplished by simultaneous precipitation of $Cu(OH)_2(s)$ and adsorption of $Cu(OH)^+$ and $Cu(OH)_3^-$ on MWCNTs.

The finial pH values against the initial pH values are also plotted in Fig. 2. The solid line represents that the pH values do not change during the adsorption process. However, one can see that the finial pH was lower than the initial pH with a value which decreased with increasing of the initial pH. The decrease of pH may be attributed to the release of H^+ from the surface of MWCNTs into solution. With the increasing of solution pH, the degree of deprotonation of MWCNT surfaces increased, thus more metal ions were adsorbed and more H^+ ions were released into solution, which resulted in the decrease of pH values after Cu(II) adsorption [37].

The effect of the background electrolyte concentrations on Cu(II) adsorption to MWCNTs in wide pH range is fairly negligible (Fig. 2). The results of ionic-strength effect on Cu(II) adsorption are consistent with those reported in the literature [38]. The background electrolyte concentration influences the thickness and interface potential of the double layer, affecting the binding of the adsorbing species. The background electrolyte ions are placed in the same plane as the outer-sphere complexes, thus, outer-sphere complexes are expected to be more susceptible to ionic-strength variations than inner-sphere complexes. Consequently, the adsorption of Cu(II) may imply the formation of inner-sphere complexes on the surfaces of MWCNTs. Hayes and Leckie [39] proposed that the influence of the background electrolyte on the adsorption reaction can be applied to predict the adsorption reaction. β-plane adsorption can be assumed to proceed when the background electrolyte easily influences the adsorption reaction; otherwise, o-plane adsorption may occur. The results of this work suggests that Cu(II) participates in an o-plane complex reaction, without being affected by the β-plane complex reaction of the background electrolyte (i.e., Na^+ and NO_3^-). The ionic strength independent and pH dependent of Cu(II) adsorption on MWCNTs indicate that the adsorption mechanism of Cu(II) is inner-sphere surface complexation at low pH values, whereas the removal of Cu(II) is accomplished

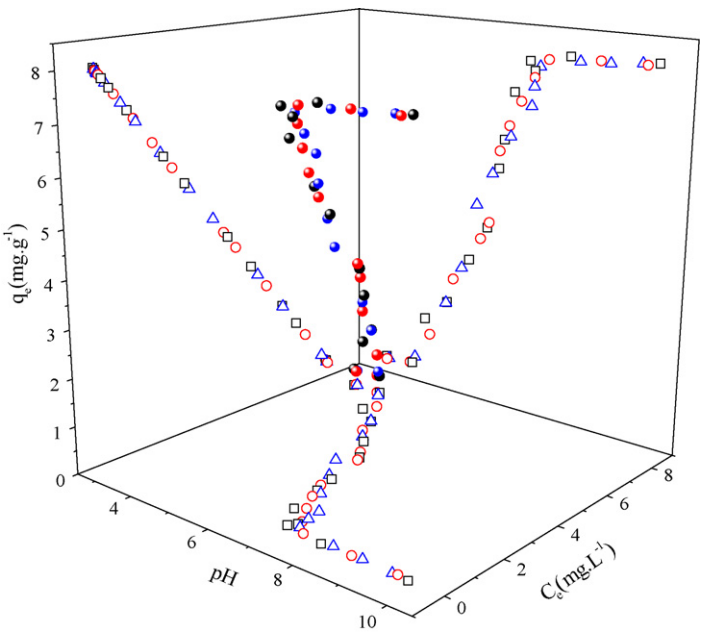

Fig. 3. 3D plots of pH, C_e and q_e of the adsorption of Cu(II) on MWCNTs. MWCNT content = 1.0 g L^{-1}, initial Cu(II) concentration = 8.0 mg L^{-1}, T = 293 K, (□) 0.1 mol L^{-1} $NaNO_3$; (○) 0.01 mol L^{-1} $NaNO_3$; (△) 0.001 mol L^{-1} $NaNO_3$.

by simultaneous precipitation and inner-sphere surface complexation at high pH values.

To illustrate the variation and relationship of pH, C_e, and q_e (mg g^{-1}, the concentration of Cu(II) on solid phase), experimental data of Cu(II) adsorption in 0.1, 0.01 and 0.001 mol L^{-1} $NaNO_3$ were plotted as 3D plots of pH, C_e, and q_e (see Fig. 3). On the pH–q_e plane, the lines are very similar to that of pH-adsorption percentage (see Fig. 2); On the pH–C_e plane, the projection on the pH–C_e plane is just the inverted image of the projection on the pH-q_e plane; On the C_e–q_e plane, the projection is a straight line containing all experimental data. It is well known that the initial concentration of Cu(II) in each experimental point is the same. The following equation can describe the relationship of C_e–q_e:

$$VC_0 = mq_e + VC_e \quad (1)$$

Eq. (1) can be rearranged as:

$$q_e = C_0\frac{V}{m} - C_e\frac{V}{m} \quad (2)$$

where V is the volume and m is the mass of MWCNTs. Thereby, the experimental data of C_e–q_e lies in a straight line with a lope ($-V/m$) and intercept (C_0V/m). The slope and intercept calculated from the C_e–q_e line are −1.0 and 8.0, which are quite in accordance with the values of V/m = 1.0 (L g^{-1}) and C_0V/m = 8.0 (mg g^{-1} × L g^{-1}) (i.e., the values calculated from V/m = 1.0 L g^{-1} and C_0 = 8.0 mg g^{-1}). The 3D plots show the relationship of pH, C_e, and q_e very clearly, i.e., all the data of C_e–q_e lie in a straight line with slope $-V/m$ and intercept C_0V/m for the same initial concentration of Cu(II) and the same MWCNTs content.

3.3. Effect of HA/FA

Fig. 4 shows the pH dependent of Cu(II) adsorption on MWCNTs in the absence and presence of HA/FA. As it is illustrated in Fig. 4, a positive effect of HA/FA on Cu(II) adsorption to MWCNTs is observed at low pH values, while a negative effect of HA/FA on Cu(II) adsorption to MWCNTs is observed at high pH values. Fig. 5 shows the adsorption of HA and FA on MWCNTs as a function of pH, it can be clearly found that about (90 ± 2%) HA/FA is adsorbed

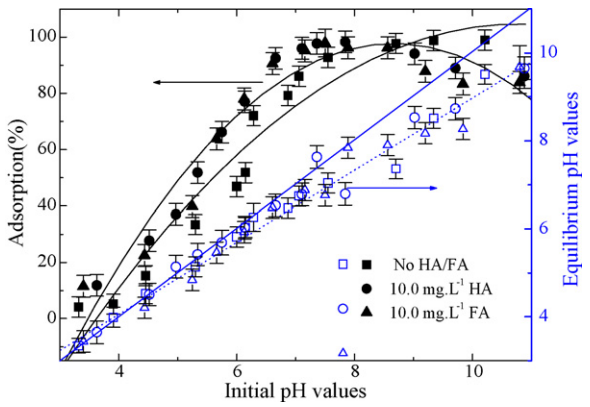

Fig. 4. Effect of HA/FA on Cu(II) adsorption on MWCNTs as a function of pH. MWCNT content = 1.0 g L^{-1}, initial Cu(II) concentration = 8.0 mg L^{-1}, I = 0.01 mol L^{-1} $NaNO_3$, T = 293 K. Solid points: adsorption vs. initial pH values; open points: equilibrium pH values vs. initial pH values.

on MWCNTs at pH <7.5, and then the adsorption decreases with increasing pH. Ghosh et al. [40] and Yang and Xing [23] measured the zeta potentials of HA and FA as a function of pH, respectively, and it was reported that both HA and FA were negatively charged in the pH range of 3.0–10.0. The observations are in agreement with our potentiometric titration results. Therefore, at low pH values, the negatively charged HA/FA can be easily adsorbed on the positively charged surfaces of MWCNTs because of the electrostatic attraction, the strong complexation ability of surface adsorbed HA/FA with Cu(II) results in the enhancement of Cu(II) adsorption on MWCNTs at low pH values. However, at high pH values, the adsorption of the negatively charged HA/FA on the negatively charged surfaces of MWCNTs becomes difficult because of the electrostatic repulsion, thus, the HA/FA in solution forms soluble complexes of HA/FA–Cu(II) in solution, and thereby results in the reducing of Cu(II) adsorption on MWCNTs.

It is very interesting to find that the adsorption curve of Cu(II) on MWCNTs in the presence of HA is quite similar to that of Cu(II) in the presence of FA. HA and FA are chemically heterogeneous compounds containing different types of functional groups at different proportions and configurations. HA and FA contain carboxyl groups, amine groups and phenolic groups [28], and these functional groups play an important role in affecting Cu(II) adsorption on MWCNTs. The samples of HA and FA are extracted from the same soil samples and they have similar functional groups such as car-

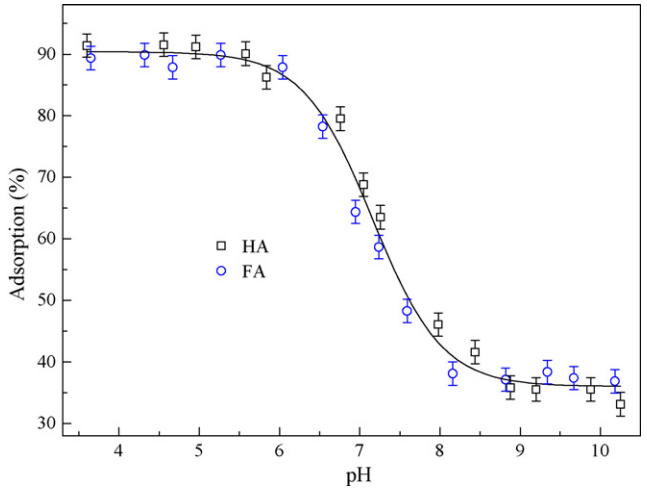

Fig. 5. Sorption of HA and FA on MWCNTs as a function of pH. $C_{(HA/FA)}$ = 10.0 mg L^{-1}, MWCNT content = 1.0 g L^{-1}, I = 0.01 mol L^{-1} $NaNO_3$, T = 293 K.

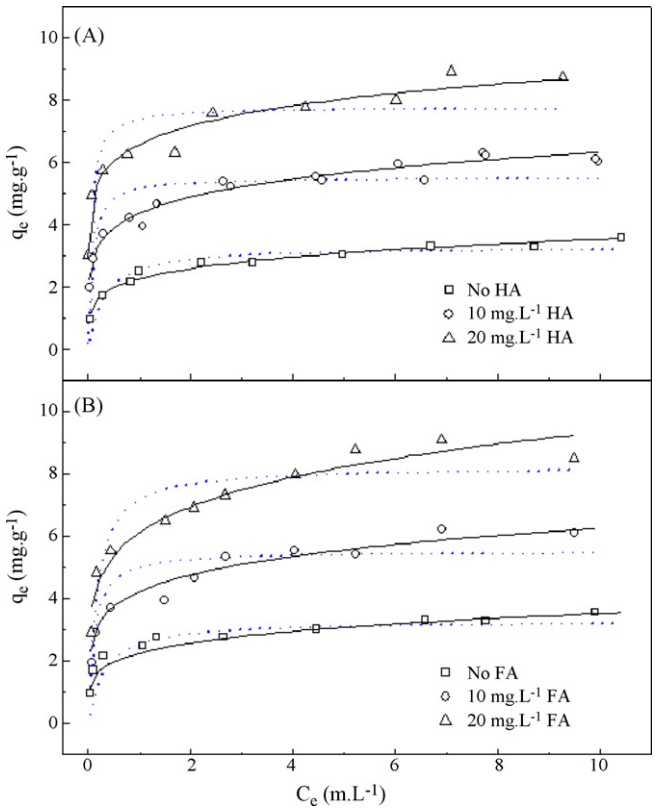

Fig. 6. Effect of HA/FA initial concentrations on Cu(II) adsorption on MWCNTs. MWCNT content = 1.0 g L^{-1}, T = 293 K, pH: 5.95 ± 0.05, I = 0.01 mol L^{-1} $NaNO_3$, A: in the presence of HA; B: in the presence of FA. Symbols denote experimental data, dot lines represent the model fitting of Langmuir equation, solid lines represent the model fitting of Freundlich equation.

boxyl and phenolic groups. It is obvious in Fig. 5 that the adsorption behavior of HA is very similar to that of FA. These similar functional groups and adsorption behavior of HA and FA may interpret the similar adsorption curve of Cu(II) on MWCNTs in the presence of HA/FA.

The equilibrium pH values are also plotted as a function of initial pH values for each experimental data (Figs. 2 and 4). One can see that the final pH value is lower than the initial pH value, and this difference becomes higher for higher adsorption percentage of Cu(II) on MWCNTs. The pH decreasing after Cu(II) adsorption suggests that part of H^+ is released from MWCNTs to solution [37].

The adsorption isotherms of Cu(II) on MWCNTs at pH 5.95 ± 0.05 in the absence and presence of HA/FA are shown in Fig. 6. For isotherm modeling, herein, both the Langmuir and the Freundlich isotherm models were employed to describe the adsorption characteristics of Cu(II) on MWCNTs.

The Langmuir model can be represented by the following equation:

$$q_e = \frac{bq_{\max}C_e}{1 + bC_e} \quad (3)$$

Eq. (3) can be expressed in the linear form:

$$\frac{1}{q_e} = \frac{1}{q_{\max}} + \frac{1}{bq_{\max}}\frac{1}{C_e} \quad (4)$$

where $q_{\max}$ (mg g^{-1}) and b (L g^{-1}) are the Langmuir constants related to the adsorption capacity and adsorption energy, respectively.

The Freundlich model has the following form:

$$q_e = k_F C_e{}^n \quad (5)$$

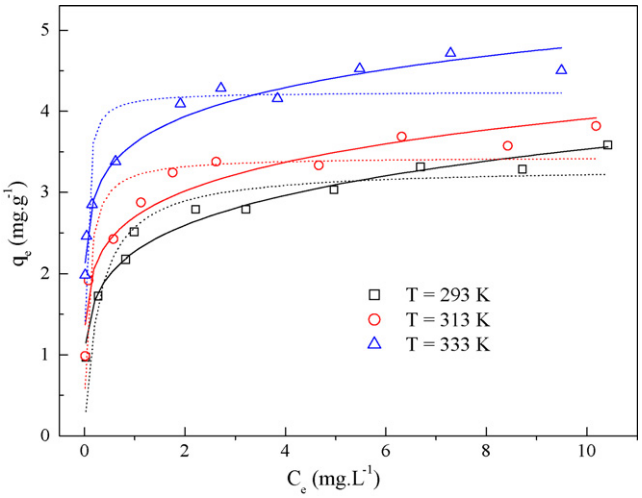

Fig. 7. Adsorption isotherms of Cu(II) on MWCNTs at three different temperatures. MWCNT content = 1.0 g L^{-1}, pH: 5.95 ± 0.05, I = 0.01 mol L^{-1} $NaNO_3$, symbols denote experimental data, dot lines represent the model fitting of Langmuir equation, solid lines represent the model fitting of Freundlich equation.

Eq. (5) can also be expressed in the linear form:

$$\log\ q_e = \log\ k_F + n\ \log\ C_e \quad (6)$$

where k_F (mg^{1-n} g^{-1} L^n) represents the adsorption capacity and n represents the degree of dependence of adsorption at equilibrium concentration.

The Langmuir and Freundlich constants are obtained from fitting the isotherm model to the adsorption equilibrium data and given in Tables 3A and 3B. The R^2 values of the Freundlich model are much higher than those of the Langmuir model, indicating that the Freundlich model fits the adsorption data better than the Langmuir model. It is generally regarded that metal ion adsorption equilibrium data can be commonly correlated with the Langmuir or the Freundlich isotherm models [41–43]. The Langmuir isotherm model is valid for dynamic equilibrium adsorption process on completely homogenous surfaces whereas the Freundlich isotherm model is applicable to heterogeneous surface. The adsorption of metal ions on MWCNTs can be well described by both Langmuir and Freundlich isotherm model [34,44,45]. Xu et al. [35] and Li et al. [46] have studied the adsorption of Pb(II) on MWCNTs, respectively, and reported that the adsorption can be well correlated by the Freundlich isotherm model. Some other researchers stated that metal ion adsorption on MWCNTs followed the Langmuir isotherm model [17,47–52]. The results found in this work are identical to those reported in the references [35,46,47].

Fig. 6 also shows the influence of HA/FA initial concentrations on Cu(II) adsorption onto MWCNTs. From Fig. 6, one can see that adsorption isotherms of Cu(II) at higher initial HA/FA concentrations are higher than those of Cu(II) at lower FA/HA concentrations. At higher concentrations of HA/FA, more functional groups, such as phenolic and carboxylic groups, are available to form strong complexes with Cu(II), and results in more Cu(II) ions to be adsorbed on FA/HA–MWCNT hybrids. The different addition sequences of FA/HA and Cu(II) to MWCNT suspensions on Cu(II) adsorption are also studied and the results show that no difference is found in Cu(II) adsorption in the ternary systems of the three addition sequences (Figure SI-6).

3.4. Adsorption thermodynamics

The adsorption isotherms of Cu(II) on MWCNTs at T = 293, 313 and 333 K are shown in Fig. 7. The adsorption isotherm is the highest at T = 333 K and is the lowest at T = 293 K, indicating that the

Table 3A
The parameters of Langmuir isotherm fitting of Cu(II) adsorption on MWCNTs.

Conditions	Langmuir parameters		
	q_{max} (mg g^{-1})	b	R^2
Cu(II)–MWCNTs (T = 293 K)	3.309 ± 0.167	3.466 ± 1.136	0.864
Cu(II)–MWCNTs (T = 313 K)	3.439 ± 0.141	13.559 ± 4.930	0.868
Cu(II)–MWCNTs (T = 333 K)	4.239 ± 0.177	33.036 ± 10.819	0.861
Cu(II)–MWCNTs–10 mg L^{-1} HA (T = 293 K (batch 1))	5.524 ± 0.291	14.087 ± 5.917	0.886
Cu(II)–MWCNTs–10 mg L^{-1} FA (T = 293 K (batch 1))	5.540 ± 0.272	9.830 ± 3.473	0.824
Cu(II)–MWCNTs–20 mg L^{-1} HA (T = 293 K)	7.776 ± 0.538	19.177 ± 12.274	0.853
Cu(II)–MWCNTs–20 mg L^{-1} FA (T = 293 K)	8.246 ± 0.336	16.788 ± 4.867	0.868
Cu(II)–MWCNTs–10 mg L^{-1} HA (T = 293 K (batch 2))	6.004 ± 0.506	3.120 ± 1.760	0.816
Cu(II)–MWCNTs–10 mg L^{-1} FA (T = 293 K (batch 2))	5.827 ± 0.424	6.073 ± 3.123	0.817
Cu(II)–MWCNTs–10 mg L^{-1} HA (T = 293 K (batch 3))	6.458 ± 0.391	2.259 ± 0.630	0.866
Cu(II)–MWCNTs–10 mg L^{-1} FA (T = 293 K (batch 3))	6.190 ± 0.244	4.331 ± 1.026	0.913

Table 3B
The parameters of Freundlich isotherm fitting of Cu(II) adsorption on MWCNTs.

Conditions	Freundlich parameters		
	k_F (mg^{1-n} g^{-1} L^n)	n	R^2
Cu(II)–MWCNTs (T = 293 K)	2.270 ± 0.054	0.192 ± 0.014	0.974
Cu(II)–MWCNTs (T = 313 K)	2.696 ± 0.082	0.177 ± 0.020	0.941
Cu(II)–MWCNTs (T = 333 K)	3.608 ± 0.053	0.125 ± 0.008	0.977
Cu(II)–MWCNTs–10 mg L^{-1} HA (T = 293 K (batch 1))	4.372 ± 0.064	0.160 ± 0.008	0.986
Cu(II)–MWCNTs–10 mg L^{-1} FA (T = 293 K (batch 1))	4.240 ± 0.111	0.170 ± 0.015	0.958
Cu(II)–MWCNTs–20 mg L^{-1} HA (T = 293 K)	6.581 ± 0.119	0.124 ± 0.010	0.968
Cu(II)–MWCNTs–20 mg L^{-1} FA (T = 293 K)	6.127 ± 0.186	0.184 ± 0.019	0.942
Cu(II)–MWCNTs–10 mg L^{-1} HA (T = 293 K (batch 2))	4.369 ± 0.136	0.156 ± 0.018	0.942
Cu(II)–MWCNTs–10 mg L^{-1} FA (T = 293 K (batch 2))	4.149 ± 0.151	0.213 ± 0.022	0.947
Cu(II)–MWCNTs–10 mg L^{-1} HA (T = 293 K (batch 3))	4.088 ± 0.121	0.226 ± 0.019	0.962
Cu(II)–MWCNTs–10 mg L^{-1} FA (T = 293 K (batch 3))	4.295 ± 0.213	0.213 ± 0.022	0.988

adsorption of Cu(II) on MWCNTs is more pronounced at higher temperature.

The thermodynamic parameters (ΔH°, ΔS°, and ΔG°) for Cu(II) adsorption on MWCNTs can be calculated from the temperature-dependent adsorption. The values of standard enthalpy change (ΔH°) and standard entropy change (ΔS°) can be calculated from the slope and y-intercept of the plot of $\ln K_d$ vs. $1/T$ (Fig. SI-7) using the following equations:

$$K_d = \frac{C_0 - C_e}{C_e}\frac{V}{m} \quad (7)$$

$$\ln K_d = \frac{\Delta S^\circ}{R} - \frac{\Delta H^\circ}{RT} \quad (8)$$

where C_0 is the initial concentration (mg L^{-1}), C_e is the equilibration concentration after centrifugation (mg L^{-1}), V is the volume (mL) and m is the mass of MWCNTs (g), R (8.314 J mol^{-1} K^{-1}) is the ideal gas constant, and T (K) is the temperature in Kelvin.

Gibbs free energy changes (ΔG°) of specific adsorption are calculated from:

$$\Delta G^\circ = \Delta H^\circ - T\Delta S^\circ \quad (9)$$

Relevant parameters calculated from Eqs. (8) to (9) are given in Table 4. The determination of thermodynamic parameters provides an insight into the mechanism concerning the adsorptive interaction of Cu(II) with MWCNTs. It is clear that the values of ΔH° are positive, i.e., the adsorption process is endothermic. One possible interpretation of the endothermic process is that Cu(II) ions are well solvated in water. In order for Cu(II) ions to adsorb, they are denuded of their hydration sheath to some extent, and this dehydration process need energy. It is assumed that this energy of dehydration exceed the exothermicity of Cu(II) ions attaching to MWCNTs surface. The removal of water molecules from Cu(II) ions is essentially an endothermic process, and the endothermicity of the desolvation process exceed the enthalpy of adsorption to a considerable extent. The Gibbs free energy change (ΔG°) is negative as expected for a spontaneous process under our experimental conditions. The decrease of ΔG° with the increase of temperature indicates more efficient adsorption at higher temperature. At higher temperature, Cu(II) ions are readily desolvated, and thereby their adsorption becomes more favorable. The positive values of entropy change (ΔS°) reflect the affinity of MWCNTs towards Cu(II) ions in aqueous solutions and might suggest some structure changes [53]. In previous studies, the thermodynamic parameters of oxidized MWCNTs for adsorption of heavy metal ions, such as Cd(II), Ni(II), Pb(II), Zn(II), Eu(III), Th(IV) and Cr(VI) from aqueous solutions have been extensively investigated [13,17,28,33–37,45,46]. The results revealed that the enthalpy change (ΔH°) and entropy change (ΔS°) are positive indicating the endothermic nature of the adsorption process and the increase of randomness at the solid/liquid interface during the adsorption process, while the negative free energy change (ΔG°) suggests that the adsorption process is spontaneous. The thermodynamic parameters are identical to those reported in the literatures [13,17,18,33–37,45,46].

Table 4
Thermodynamic parameters for Cu(II) adsorption on MWCNTs.

C_0 (mg L^{-1})	ΔH° (kJ mol^{-1})	ΔS° (J mol^{-1} K^{-1})	ΔG° (kJ mol^{-1})		
			293 K	313 K	333 K
2.0	61.38	281.32	−21.09	−87.81	−93.74
6.0	18.18	118.08	−16.44	−36.86	−39.35
10.0	10.24	86.26	−15.05	−26.93	−28.75
14.0	6.42	70.26	−14.18	−21.93	−23.42

4. Conclusions

From the results of Cu(II) adsorption on MWCNTs under our experimental conditions, the following conclusions can be obtained:

(1) The adsorption of Cu(II) on MWCNTs is strongly dependent on pH values in the range of 3.0–10.0. The adsorption of Cu(II) on MWCNTs increases with pH increasing from 3.0 to 7.5, and then maintains high level at pH >7.5.
(2) The adsorption of Cu(II) on MWCNTs is independent of ionic strength in the wide pH range. The adsorption of Cu(II) is mainly dominated by inner-sphere surface complexation at low pH values, whereas the adsorption is accomplished by precipitation and inner-sphere surface complexation at high pH values.
(3) The adsorption isotherms of Cu(II) on MWCNTs can be described well by both the Langmuir and Freundlich model, and the Freundlich model fits the adsorption data better than the Langmuir model.
(4) The thermodynamic data derived from temperature-dependent adsorption isotherms suggest that the adsorption reaction is spontaneous and is enhanced at higher temperature.
(5) The adsorption of Cu(II) is influenced by HA/FA significantly, and the effect of HA/FA on Cu(II) adsorption is dependent on pH values. The adsorption is enhanced at low pH values and is reduced at high pH values.
(6) Results of this work are of great importance for environmental application of MWCNTs in the treatment and removal of metal ions from large volume of aqueous solutions.

Acknowledgement

Financial supports from the National Natural Science Foundation of China (20971126; 20907055), Knowledge Innovation Program of CAS, 973 project (2007CB936602), the Open Fund of State Key Laboratory of Estuarine and Coastal Research and Special Foundation for High-level Waste Disposal (2007-840) are acknowledged.

Appendix A. Supplementary data

Supplementary data associated with this article can be found, in the online version, at doi:10.1016/j.jhazmat.2010.01.084.

References

[1] S. Iijima, Helical microtubules of graphitic carbon, Nature 354 (1991) 56–58.
[2] S. Iijima, T. Ichihashi, Single-shell carbon nanotubes of 1-nm diameter, Nature 363 (1993) 603–605.
[3] N. Jonge, Y. Lamy, K. Schoots, T.H. Oosterkamp, High brightness electron beam from a multi-walled carbon nanotube, Nature 420 (2002) 393–395.
[4] M.S. Dresselhaus, I.L. Thomas, Alternative energy technologies, Nature 414 (2001) 332–337.
[5] P.G. Collins, K. Bradley, M. Ishigami, A. Zettl, Extreme oxygen sensitivity of electronic properties of carbon nanotubes, Science 287 (2000) 1801–1804.
[6] A.C. Dillon, K.M. Jones, T.A. Bekkedahl, C.H. Kiang, D.S. Bethune, M.J. Heben, Storage of hydrogen in single-walled carbon nanotubes, Nature 386 (1997) 377–379.
[7] C. Liu, Y.Y. Fan, M. Liu, H.T. Cong, H.M. Cheng, M.S. Dresselhaus, Hydrogen storage in single-walled carbon nanotubes at room temperature, Science 286 (1999) 1127–1129.
[8] L. Schlapbach, A. Züttel, Hydrogen-storage materials for mobile applications, Nature 414 (2001) 353–358.
[9] M.S. Mauter, M. Elimelech, Environmental applications of carbon-based nanomaterials, Environ. Sci. Technol. 42 (2008) 5843–5859.
[10] J. Wang, C. Timchalk, Y. Lin, Carbon nanotube-based electrochemical sensor for assay of salivary cholinesterase enzyme activity: an exposure biomarker of organophosphate pesticides and nerve agents, Environ. Sci. Technol. 42 (2008) 2688–2693.
[11] C.W. Lam, J.T. James, R. McCluskey, S. Arepalli, R.L. Hunter, A review of carbon nanotube toxicity and assessment of potential occupational and environmental health risks, Crit. Rev. Toxicol. 36 (2006) 189–217.
[12] B. Nowack, T.D. Bucheli, Occurrence, Behavior and effects of nanoparticles in the environment, Environ. Pollut. 150 (2007) 5–22.
[13] G.P. Rao, C. Lu, F. Su, Sorption of divalent metal ions from aqueous solution by carbon nanotubes: a review, Sep. Purif. Technol. 58 (2007) 224–231.
[14] B. Pan, B.S. Xing, Adsorption mechanisms of organic chemicals on carbon nanotubes, Environ. Sci. Technol. 42 (2008) 9005–9013.
[15] M. Tuzen, M. Soylak, Multiwalled carbon nanotubes for speciation of chromium in environmental samples, J. Hazard. Mater. 147 (2007) 219–225.
[16] M. Tuzen, K.O. Saygi, C. Usta, M. Soylak, Pseudomonas aureginosa immobilized multiwalled carbon nanotubes as biosorbent for heavy metal ions, Bioresour. Technol. 99 (2008) 1563–1570.
[17] C. Lu, H. Chiu, C. Liu, Removal of zinc(II) from aqueous solution by purified carbon nanotubes: kinetics and equilibrium studies, Ind. Eng. Chem. Res. 45 (2006) 2850–2855.
[18] C. Lu, C. Liu, G.P. Rao, Comparisons of sorbent cost for the removal of Ni^{2+} from aqueous solution by carbon nanotubes and granular activated carbon, J. Hazard. Mater. 151 (2008) 239–246.
[19] G.C. Chen, X.Q. Shan, Y.S. Wang, Z.G. Pei, X.E. Shen, B. Wen, G. Owens, Effects of copper, lead, and cadmium on the sorption and desorption of atrazine onto and from carbon nanotubes, Environ. Sci. Technol. 42 (2008) 8297–8302.
[20] G.C. Chen, X.Q. Shan, Y.S. Wang, B. Wen, Z.G. Pei, Y.N. Xie, T. Liu, J.J. Pignatello, Adsorption of 2,4,6-trichlorophenol by multi-walled carbon nanotubes as affected by Cu(II), Water Res. 43 (2009) 2409–2418.
[21] H. Hyung, J.H. Kim, Natural organic matter (NOM) adsorption to multi-walled carbon nanotubes: effect of NOM characteristics and water quality parameters, Environ. Sci. Technol. 42 (2008) 4416–4421.
[22] H. Hyung, J.D. Fortner, J.B. Hughes, J.H. Kim, Natural organic matter stabilizes carbon nanotubes in the aqueous phase, Environ. Sci. Technol. 41 (2007) 179–184.
[23] K. Yang, B. Xing, Adsorption of fulvic acid by carbon nanotubes from water, Environ. Pollut. 157 (2009) 1095–1100.
[24] X.L. Wang, J.L. Lu, B.S. Xing, Sorption of organic contaminants by carbon nanotubes: influence of adsorbed organic matter, Environ. Sci. Technol. 42 (2008) 3207–3212.
[25] J.F. Colomer, P. Piedigrosso, I. Willems, C. Journet, P. Bernier, G. van Tendeloo, A. Fonseca, J.B. Nagy, Pruification of catalytically produced multi-wall nanotubes, J. Chem. Soc. Faraday Trans. 94 (1998) 3753–3758.
[26] A.G. Rinzler, J. Liu, H. Dai, P. Nikolaev, C.B. Huffman, F.J. Rodriguez-Macias, P.J. Boul, A.H. Lu, D. Heymann, D.T. Colbert, R.S. Lee, J.E. Fischer, A.M. Rao, P.C. Eklund, R.E. Smalley, Large-scale purification of single-wall carbon nanotubes: process, product, and characterization, Appl. Phys. A 67 (1998) 29–37.
[27] D. Aggarwal, M. Goyal, R.C. Bansal, Adsorption of chromium by activated carbon from aqueous solution, Carbon 37 (1999) 1989–1997.
[28] X.L. Tan, X.K. Wang, H. Geckeis, T. Rabung, Sorption of Eu(III) on humic acid or fulvic acid bound to alumina studied by SEM-EDS, XPS, TRLFS and batch techniques, Environ. Sci. Technol. 42 (2008) 6532–6537.
[29] Z.Y. Tao, J. Zhang, J. Zhai, Characterization and differentiation of humic acids and fulvic acids in soils from various regions of China by nuclear magnetic resonance spectroscopy, Anal. Chim. Acta 395 (1999) 199–203.
[30] J. Zhang, J. Zhai, F.Z. Zhao, Z.Y. Tao, Study of soil humic substances by cross-polarization magic angle spinning ^{13}C nuclear magnetic resonance and pyrolysis-capillary gas chromatography, Anal. Chim. Acta 378 (1999) 177–182.
[31] Y.P. Chin, G. Alken, E. O'Loughlin, Molecular weight, polydispersity, and spectroscopic properties of aquatic humic substances, Environ. Sci. Technol. 28 (1994) 1853–1858.
[32] B. Lee, D. Lu, J.N. Kondo, K. Domen, Three-dimensionally ordered mesoporous niobium oxide, J. Am. Chem. Soc. 124 (2002) 11256–11257.
[33] Y.H. Li, S. Wang, Z. Luan, J. Ding, C. Xu, D. Wu, Adsorption of cadmium(II) from aqueous solution by surface oxidized carbon nanotubes, Carbon 41 (2003) 1057–1062.
[34] Y.H. Li, S. Wang, J. Wei, X. Zhang, C. Xu, Z. Luan, D. Wu, B. Wei, Lead adsorption on carbon nanotubes, Chem. Phys. Lett. 357 (2002) 263–266.
[35] D. Xu, X.L. Tan, C.L. Chen, X.K. Wang, Removal of Pb(II) from aqueous solution by oxidized multi-walled carbon nanotubes, J. Hazard. Mater. 154 (2008) 407–417.
[36] C. Lu, H. Chiu, Chemical modification of multiwalled carbon nanotubes for sorption of Zn^{2+} from aqueous solution, Chem. Eng. J. 139 (2008) 462–468.
[37] X.K. Wang, C.L. Chen, W.P. Hu, A.P. Ding, D. Xu, X. Zhou, Sorption of $^{243}Am(III)$ to multi-wall carbon nanotubes, Environ. Sci. Technol. 39 (2005) 2856–2860.
[38] C.H. Wu, Studies of the equilibrium and thermodynamics of the adsorption of Cu^{2+} onto as-produced and modified carbon nanotubes, J. Colloid Interface Sci. 311 (2007) 338–346.
[39] K.F. Hayes, J.O. Leckie, Modeling ionic strength effects on cation adsorption at hydrous oxide/solution interfaces, J. Colloid Interface Sci. 115 (1987) 564–572.
[40] S. Ghosh, H. Mashayekhi, B. Pan, P. Bhowmik, B.S. Xing, Colloidal behavior of aluminum oxide nanoparticles as affected by ph and natural organic matter, Langmuir 24 (2008) 12385–12391.
[41] M.M. Rao, A. Ramesh, G.P.C. Rao, K. Seshaiah, Removal of copper and cadmium from the aqueous solutions by activated carbon derived from ceiba pentandra hulls, J. Hazard. Mater. B 129 (2006) 123–129.
[42] M. Sekar, V. Sakthi, S. Rengaraj, Kinetics equilibrium adsorption study of lead(II) onto activated carbon prepared from coconut shell, J. Colloid Interface Sci. 279 (2004) 307–313.
[43] C.H. Weng, C.P. Huang, Adsorption characteristics of Zn(II) from dilute aqueous solution by fly ash, Colloids Surf. A 247 (2004) 137–143.
[44] Z.C. Di, J. Ding, X.J. Peng, Y.H. Li, Z.K. Luan, J. Liang, Chromium adsorption by aligned carbon nanotubes supported ceria nanoparticles, Chemosphere 62 (2006) 861–865.

[45] C. Lu, C. Liu, Removal of nickel(II) from aqueous solution by carbon nanotubes, J. Chem. Technol. Biotechnol. 81 (2006) 1932–1940.
[46] Y.H. Li, Z. Di, J. Ding, D. Wu, Z. Luan, Y. Zhu, Adsorption thermodynamic, kinetic and desorption studies of Pb^{2+} on carbon nanotubes, Water Res. 39 (2005) 605–609.
[47] A. Stafiej, K. Pyrzynska, Adsorption of heavy metal ions with carbon nanotubes, Sep. Purif. Technol. 58 (2007) 49–52.
[48] C. Lu, H. Chiu, Adsorption of zinc(II) from water with purified carbon nanotubes, Chem. Eng. Sci. 61 (2006) 1138–1145.
[49] Y.H. Li, J. Ding, Z. Luan, Z. Di, Y. Zhu, C. Xu, D. Wu, B. Wei, Competitive adsorption of Pb^{2+}, Cu^{2+} and Cd^{2+} ions from aqueous solutions by multiwalled carbon nanotubes, Carbon 41 (2003) 2787–2792.
[50] C. Chen, X. Wang, Adsorption of Ni(II) from aqueous solution using oxidized multiwall carbon nanotubes, Ind. Eng. Chem. Res. 45 (2006) 9144–9149.
[51] C.L. Chen, X.L. Li, D.L. Zhao, X.L. Tan, X.K. Wang, Adsorption kinetic, thermodynamic and desorption studies of Th(IV) on oxidized multi-wall carbon nanotubes, Colloids Surf. A 302 (2007) 449–454.
[52] Q.H. Fan, D.D. Shao, J. Hu, C.L. Chen, W.S. Wu, X.K. Wang, Adsorption of humic acid and Eu(III) to multi-walled carbon nanotubes: effect of pH, ionic strength and counterion effect, Radiochim. Acta 97 (2009) 141–148.
[53] H. Genc-Fuhrman, J.C. Tjell, D. Mcconchie, Adsorption of arsenic from water using activated neutralized red mud, Environ. Sci. Technol. 38 (2004) 2428–2434.